# Testing the suitability of metallic iron for environmental remediation: Discoloration of methylene blue in column studies

Btatkeu K. B.D.[a,b], Miyajima K.[c], Noubactep C.*[c,d], Caré S.[a]

[a] Université Paris-Est, Laboratoire Navier (UMR 8205), CNRS, ENPC, IFSTTAR, F-77455 Marne-la-Vallée, France;

[b] ENSAI/University of Ngaoundere, BP 455 Ngaoundere, Cameroon;

[c] Angewandte Geologie, Universität Göttingen, Goldschmidtstraße 3, D - 37077 Göttingen, Germany;

[d] Kultur und Nachhaltige Entwicklung CDD e.V., Postfach 1502, D - 37005 Göttingen, Germany.

(*) Correspond author; e-mail: cnoubac@gwdg.de; Tel. +49 551 39 3191, Fax. +49 551 399379.

## Abstract

A new method to correlate intrinsic reactivity and treatability efficiency of metallic iron ($Fe^0$) was evaluated. A 2.0 mg $L^{-1}$ methylene blue (MB) solution was used in gravity fed column experiments. The intrinsic reactivity of nine $Fe^0$ materials (ten samples) was characterized using the EDTA test. Three commercial $Fe^0$ materials ZVI1 (0.40 - 0.80 mm), ZVI9 (0.50 mm) and ZVI10 (0.45 - 0.55 mm) were tested in column experiments. A layer containing 100 g of $Fe^0$ was sandwiched between 19.0 to 20.0 cm upper coarse sand (1.6 - 2.0 mm) and 8.0 cm lower fine sand (0.25 - 0.30 mm). 500 mL of the MB solution was daily filtered through each column for one month. Effluent solutions were characterized for MB and Fe concentrations. The columns were also characterized by the evolution of the hydraulic conductivity (k values). Results showed (i) quantitative MB removal (> 88 %) and (ii) limited Fe release for all three columns. After about 25 days, the Fe levels were constantly less than 1.0 mg $L^{-1}$. The most significant difference was observed in the evolution of the k value and was attributed to the different material sorting. Less sorted ZVI1 exhibited the lowest initial k value (8.0 vs 43.0 mm $min^{-1}$ for ZVI9 and ZVI10) and most significant permeability loss. Results confirmed the usefulness of the tested protocol as a reliable method to assess the efficiency of $Fe^0$ materials in short term column experiments. Well-sorted $Fe^0$ materials are recommended for long term efficient $Fe^0$ filtration systems.

**Keywords:** Intrinsic reactivity, Methylene blue, Reactive filtration, Treatability efficiency, Zerovalent iron.

## 1 Introduction

Metallic iron ($Fe^0$) is a reactive material currently used for environmental remediation and safe drinking water provision [1-7]. Available $Fe^0$ materials are obtained from various sources [8-12] and are supposed to satisfy design expectations [7,13-17]. However, there is no standard method to access the suitability of $Fe^0$ materials for individual applications. As a rule, used materials are characterized: (i) by selected physical and chemical parameters (e.g. elemental composition, particle size, surface area) and (ii) for their ability to remove the specific species of interest (efficiency in treatability studies) [11,18,19]. However, each reactive material should be primarily characterized by its intrinsic reactivity.

The 'intrinsic reactivity' is a material-dependent but system-independent qualitative trend. The 'removal efficiency' or 'treatability efficiency' is a system-dependent quantifiable parameter. For a reactive material like $Fe^0$, the intrinsic reactivity should be correlated to the treatability efficiency. For activated carbons (an inert material) several indicators for the treatability efficiency have been introduced including the iodine number, the phenol number, the methylene blue number and the tannic acid number [20]. Appropriate treatability indicators for $Fe^0$ are urgently needed.

The intrinsic reactivity could be regarded as the most important characteristic in selecting $Fe^0$ for designing filtration systems. Under specific operational conditions, intrinsic reactivity characterizes the kinetics of the process of iron oxidative dissolution in the absence of any mass transfer restrictions [21]. The extent of iron corrosion depends primarily on the solubility of iron under the operational conditions. For example, in the presence of some solutes (e.g. organic complexants), aqueous iron forms soluble chelates and $Fe^0$ tend to dissolve at constant rate. Others solutes (e.g. $PO_4^{3-}$ ions) produce relatively insoluble chelates

54 which form a coating over the metal and tend to stifle iron corrosion [22]. Despite this general
55 trend, one could not state that a $Fe^0$ specimen is not suitable for $PO_4$-contaminated waters for
56 example. The suitability of $Fe^0$ for any polluted water depends on at least three interrelated
57 operational parameters: (i) the $Fe^0$ intrinsic reactivity, (ii) the nature and the extent of the
58 contamination and (iii) the water flow velocity (contact time, filter thickness) [23].
59 Current approaches to design $Fe^0$-based filtration systems suggest that the intrinsic reactivity
60 is not optimised in respect of the most site-specific effective material. The reasons are that the
61 importance of intrinsic reactivity and its relationship with other operational parameters are not
62 yet fully appreciated and/or understood in engineering practice. Relevant operational
63 parameters include: (i) hydraulic characteristics, (ii) shape, size and surface characteristics
64 used $Fe^0$ material and non-expansive additives (e.g. gravel, pumice, sand), (ii) compactness or
65 porosity of the filter [24-26]. In recent years, significant progress has been made in
66 characterizing the intrinsic reactivity of $Fe^0$ materials in water by $H_2$ evolution [27-30] and
67 iron dissolution in EDTA (EDTA test) [11,21,31,32]. Achieved results were contrasted with
68 results from the removal of uranium [31,33], discoloration of methylene blue [34] and
69 removal of arsenic [35]. Available data validate the suitability of the EDTA test to
70 characterize the intrinsic reactivity of $Fe^0$ materials.
71 The present study extends this effort by relating the intrinsic reactivity, the $Fe^0$ particle
72 size/shape and the hydraulic conductivity of $Fe^0$ filters for three selected materials. A total of
73 9 $Fe^0$ materials making up 10 samples (ZVI1 through ZVI10) have been characterized by the
74 EDTA test. Three selected $Fe^0$ materials (ZVI1, ZVI9, ZVI10) were then used in column
75 studies to characterize the evolution of (i) Fe release, (ii) methylene blue (MB) discoloration
76 and (iii) hydraulic conductivity. A 2.0 mg $L^{-1}$ MB solution was used as an indictor for the
77 impact of iron corrosion on the filtration process.

## 2 Background of the experimental methodology

The suitability of a pure $Fe^0$ layer (100 % $Fe^0$) in a sand column to characterize the intrinsic reactivity of $Fe^0$ materials arises mainly from the historical observation by Mitchell et al. [36] that (i) sand is a good adsorbent for methylene blue (MB) and (ii) iron oxide coated sand is less adsorptive than pure sand. Accordingly, sandwiching a layer of different $Fe^0$ in a standard sand column in parallel studies and comparing individual system's responses for MB discoloration could be an efficient tool to access $Fe^0$ intrinsic reactivity. Using a 100 % $Fe^0$ layer is a tool to shorten experimental duration as less room is left for volumetric expansive iron corrosion [37,38]. In fact, a 100 % $Fe^0$ bed has been demonstrated efficient for contaminant removal but not sustainable [1,6,39].

In this study a 19.1 to 20.0 cm coarse sand layer ($H_1$-sand, Tab. 1) is used before the pure $Fe^0$ layer and a 8.0 cm fine sand layer ($H_2$-sand) thereafter. It is expected that MB will be undisturbed discoloured in $H_1$-sand layer at the beginning of the experiment. However, a disturbance of the flow regime due to expansive iron corrosion will hindered the extent of MB discoloration in the whole column and in the $H_2$-sand layer in particular. Additionally decreased adsorptive efficiency due to in-situ iron oxide coating will impair MB discoloration. Thus, both a decreased of the hydraulic conductivity (permeability loss) and an accelerated MB breakthrough could be observed within some weeks. For materials of comparable particle size and shape, the most reactive a material, the lower the extent of MB discoloration and the more rapid the clogging (Assumption 1).

The used methodology for the investigation of the impact of $Fe^0$ characteristics (e.g. intrinsic reactivity, shape, size, sorting) on the extent of (i) MB discoloration and (ii) decrease of hydraulic permeability comprises testing the validity of Assumptions 1 by following the MB discoloration and permeability loss in the presence of tested materials. In situ generated iron corrosion products are adsorbed onto the sand surface, worsening its capacity of MB adsorption [36]. MB breakthrough is facilitated in systems with more reactive $Fe^0$.

## 3 Material and methods

### 3.1 Solutions

#### 3.1.1 Methylene blue

The used methylene blue (MB - Basic Blue 9 from Merck) was of analytical grade. The working solution was 2.0 mg $L^{-1}$. The solutions were prepared by diluting a 1000 mg $L^{-1}$ stock solution. The stock solution was prepared weekly by dissolving accurately weighted MB in tap water. MB was chosen in this study because of its known weak adsorption onto iron oxides [36,40]. The used concentration 2.0 mg $L^{-1}$ or 6.3 μM corresponds to the concentration range of natural waters (MB as model micro-pollutant).

#### 3.1.2 Iron

A standard iron solution (1000 mg $L^{-1}$) from Baker JT® was used to calibrate the spectrophotometer used for analysis. All other chemicals used were of analytical grade. In preparation for spectrophotometric analysis, ascorbic acid was used to reduce $Fe^{III}$ in solution to $Fe^{II}$. 1,10 orthophenanthroline (ACROS Organics) was used as reagent for $Fe^{II}$ complexation. Other chemicals used in this study included L(+)-ascorbic acid and L-ascorbic acid sodium salt.

### 3.2 Solid materials

#### 3.2.1 Metallic iron ($Fe^0$)

A total of 10 samples (ZVI1 through ZVI10) from 9 $Fe^0$ materials were tested. The materials were obtained from various sources, in different forms and grain sizes. The main characteristics of these materials are summarised in Tab. 2. Fig. 1 depicts micrographs of 500 mg of each sample using a portable camera (Keyence VHX-500F). No information about manufacturing processes (e.g., raw material, heat treatment) was available to assist with subsequent data interpretation. The average elemental composition of the materials as specified by the suppliers are well-documented in the literature [25,26,41] and are not repeated here.

130 It is the objective of this study to characterize the reactivity of tested materials and compare
131 the efficiency of three of them for the discoloration of methylene blue in column studies. A
132 part from the Rheinfelden material (iPutcec GmbH & Co) which was tested in two fractions,
133 all other materials were used in their typical state and form ('as received' state) in which they
134 might be used for field applications. The Rheinfelden material was tested in two fractions: (i)
135 as received (ZVI4) and (ii) the fraction between 0.40 and 0.80 mm (ZVI1). ZVI1 was used to
136 reduce variability in grain size [26] and compare the efficiency to that of ZVI9 and ZVI10 in
137 column studies.
138 ZVI1, ZVI9 and ZVI10 used in column studies are available as fillings with a particle size
139 between 0.40 and 0.8 mm (Tab. 2). ZVI10 was not quantitatively available to enable own
140 granulometric analysis. The granulometric distribution reported by Gottinger [41] was used
141 for the presentation (Tab, 2). ZVI9 is the best sorted material, ZVI10 is better sorted than
142 ZVI1 (Fig. 1).

143 **3.2.2 Sand**

144 The used sand was a natural material from Fontainebleu (France). Fontainebleu sand was
145 available in two fractions: (i) $d \leq 0.5$ mm and (ii) $0.5 \leq d$ (mm) $\leq 5.0$. The first fraction was
146 sieved and particles ranging between 0.250 and 0.300 mm were retained for the first sand
147 layer (fine sand - $H_2$-sand, Tab. 1). The second fraction was sieved and particles ranging
148 between 1.6 and 2.0 mm were retained for the second sand layer (coarse sand - $H_1$-sand).
149 Sand was used as an adsorbent because of its worldwide availability and its use as admixing
150 agent in $Fe^0/H_2O$ systems [2,7,13,15].

151 **3.3 Experimental procedure**

152 **3.3.1 EDTA test**

153 Iron dissolution was initiated by the addition of 0.1 g of each $Fe^0$ material to 50 mL of a 2.0
154 mmol $L^{-1}$ EDTA solution. Each reaction was run for ≤ 96 hours (4 days) using narrow 70 mL
155 glass beakers to hold the solutions [11,31]. The reacting samples were left undisturbed on the

laboratory bench for the duration of experimental period and were shielded from direct sunlight to minimize $Fe^{III}$-EDTA photodegradation [42]. Iron dissolution was used to characterize the reactivity of tested $Fe^0$ [11,31].

### 3.3.2 MB discoloration

Plexiglas columns of 2.6 cm inner diameter and 50 cm length were used. The column was mostly packed with sand: 8.0 cm at the bottom ($H_2$-sand) and 19.1 to 20.0 cm at top ($H_1$-sand) of the reactive layer. A reactive layer (100 % $Fe^0$) with 100 g $Fe^0$ was sandwiched between $H_1$-sand and $H_2$-sand (Fig. 2, Tab. 1). The depth of the reactive layer was 4.5 to 5.4 cm ($H_{iron}$ - Fig. 2) for the three materials. The columns were intermittently charged with a gravity driven 2.0 mg $L^{-1}$ MB solution. Five filtration events were performed each week (daily from Monday to Friday). Each filtration event used 500 mL of the MB solution. This was to mimic the intermittent filtration with household filters for the daily water need [43]. The whole experimental duration was one month. The average time needed for the filtration of the first three 50 mL (150 mL in total) was used to calculate the flow velocity at each date. The whole effluent for each filtration event was collected and analysed for MB. At certain time intervals the iron concentration was determined. The room temperature during the experiments was 22 ± 2°C, and the initial pH value of the 2.0 mg $L^{-1}$ MB was 6.8 ± 0.2.

## 3.5 Analytical methods

### 3.5.1 Solution concentrations

MB and aqueous iron concentrations were determined by a Cary 50 UV-Vis spectrophotometer (Perkin Elmer Lambda 10 UV/Vis) at a wavelength of 664.5 nm and 510.0 nm respectively. Cuvettes with 1.0 cm light path were used. The iron determination followed the 1,10 orthophenanthroline method [44,45]. The spectrophotometer was calibrated for MB concentrations ≤ 2.5 mg $L^{-1}$ and iron concentrations ≤ 10.0 mg.$L^{-1}$. The pH value was measured by combined glass electrodes (WTW Co., Germany).

### 3.5.2 Scanning electron microscope (SEM)

Particle morphology was investigated with a cold field emission SEM (type Hitachi S-34000N). The observations enable a characterization of the morphology of all materials used in column experiments (sand, ZVI1, ZVI9 and ZVI10).

## 3.6 Expression of experimental results

### 3.6.1 Kinetics of $Fe^0$ oxidative dissolution ($k_{EDTA}$ value)

Upon immersion in a EDTA solution, $Fe^0$ is oxidative dissolved and the aqueous concentration of iron ([Fe]) linearly varies as a function of time (Eq. 1) before the solution approaches saturation [11,31].

$$[Fe]_t = k_{EDTA}\, t + b \qquad (1)$$

For each $Fe^0$ material the time-dependant linear evolution of aqueous iron concentration is used to characterize the intrinsic reactivity. The linear gradient ('$k_{EDTA}$' in Eq. 1) representing the rate of iron dissolution. The $k_{EDTA}$ values were calculated using Origin 6.0. The b value, [Fe] at t = 0, is a reflect of the amount of atmospheric corrosion present at fines at the $Fe^0$ surface [11,31].

### 3.6.2 Discoloration efficiency (E value)

In order to characterize the magnitude of tested systems for MB discoloration, the discoloration efficiency (E) was calculated (Eq. 2). After the determination of the residual MB concentration (C), the corresponding percent MB discoloration (E value) was calculated as:

$$E = [1 - (C/C_0)] * 100\% \qquad (2)$$

where $C_0$ is the initial aqueous MB concentration (2.0 mg $L^{-1}$), while C gives the MB concentration after the experiment.

### 3.6.3 Relative permeability

Saturated hydraulic conductivity K (e.g. $mm.min^{-1}$) can be expressed as:

$$K = (Q/A)*(\Delta L/\Delta H) \qquad (3)$$

where Q is volumetric flow rate, A is column cross-sectional area, L is distance from the inlet of column and $\Delta H$ is the hydraulic head.

In general, exploiting Eq. (3), experimental data are used to evaluate the hydraulic gradient ($\Delta H/\Delta L$) at each time and to deduce the saturated hydraulic conductivity (K). However, estimating the initial saturated hydraulic conductivity ($K_0$) at the start of the experiment is usually sufficient to characterize the evolution of the system. The system's permeability is then characterized by the time-dependant relative hydraulic conductivity (Eq. 4):

$$k = K/K_0 \qquad (4)$$

The K value in this study corresponds to the solution flow velocity through the columns. The flow velocity was operationally defined as the time necessary for the filtration of 50 mL of the 2.0 mg $L^{-1}$ MB solution.

## 4. Results and Discussion

### 4.1 $Fe^0$ characterization

#### 4.1.1 Photomicrography

Micrographs of the tested samples evidenced differences in shapes and sizes (Fig. 1). The grain size distribution and the availability of fines are also evidenced. Relevant information from Fig. 1 can be summarized as: (i) ZVI8 and ZVI9 are the sole well-sorted materials with regular shapes, (ii) ZVI3, ZVI6, ZVI7 and ZVI10 are covered with fines (atmospheric corrosion products), (iii) the proportion of fines in ZVI6 is relatively large. It can be further seen that sieving ZVI4 to ZVI1 has resulted in a sample roughly comparable to ZVI10 in its particle size distribution. ZVI1, ZVI9, ZVI10 and used sand fractions were further characterized by scanning electron microscope (SEM). The following characteristics of $Fe^0$ materials used in column studies should be pointed out: (i) ZVI1 and ZVI10 are similar in the particle size distribution, (ii) ZVI1 and ZVI10 are poorly sorted and (iii) ZVI9 is a relatively well-sorted material.

#### 4.1.2 Scanning electron microscope (SEM)

SEM images detailing the microstructures of sand, ZVI1, ZVI9 and ZVI10 particles are shown in Fig. 3. The coarse fraction of Fontainebleu sand was sieved and the fraction 0.400 - 0.800 was used (the same fraction like ZVI1). These observations confirm that ZVI9 is roughly regular in shape while ZVI1, ZVI10 and sand particles are irregular. Sand is more regular in shape that ZVI1 and ZVI10. Micrograph's observations are confirmed by SEM images.

## 4.2 EDTA batch test

### 4.2.1 All tested materials

The calculated dissolution rates ($k_{EDTA}$) for the ten $Fe^0$ samples are displayed in Tab. 3 and vary from 13 μg $h^{-1}$ for ZVI8 to 37 μg $h^{-1}$ for ZVI10. The least reactive material (ZVI8 from Würth) was used as negative reference like in previous studies [32-34]. The most reactive material were ZVI9 (Ferblast) and ZVI10 (Peerless). The $k_{EDTA}$ values for all remaining materials varied from 23 μg $h^{-1}$ (ZVI4) to 32 μg $h^{-1}$ (ZVI3). The overall increasing order of reactivity after the $k_{EDTA}$ value is:

$$ZVI8 < ZVI4 = ZVI1 = ZVI6 < ZVI5 = ZVI7 < ZVI2 < ZVI3 < ZVI9 = ZVI10.$$

It is important to recall that this classification does not account for the presence of iron corrosion products reflected by the b values (Tab. 3). From Tab. 3 it is clear that ZVI6 exhibited the largest b value. This is consistent with the fact that ZVI6 was physically covered by fines of rusted iron (Fig. 1). The presence of atmospheric corrosion products is the main reason why a graphical comparison of materials is not suitable [11,31]. It has been shown that the EDTA test is not suitable for powdered $Fe^0$ materials and for $Fe^0$ samples containing a high proportions of fines [11].

It should be kept in mind that: (i) $Fe^0$ materials tested here are (among) the most widely used worldwide (e.g. Connelly, Peerless, Rheinfelden); (ii) there is actually not standard protocol to test the intrinsic reactivity of $Fe^0$ materials. From these two factors, it appears that this study reliably characterizes for the first time a large array of commercial materials and could

be regarded as starting point for future works aiming as establishing standard protocol for testing $Fe^0$ materials. Based on the established order of reactivity given above, the least reactive material (ZVI1 - ZVI8 was tested as negative reference) and the both most reactive materials (ZVI9 and ZVI10) were selected for column tests. The both most reactive material differ in their sorting (Fig. 1 and Fig. 3).

### 4.2.2 Materials for column studies

Fig. 4 summarizes the results of the EDTA test for materials used in column studies. It is seen that ZVI10 ($k_{EDTA}$ = 37 ± 2 μg $h^{-1}$) and ZVI9 ($k_{EDTA}$ = 36 ± 3 μg $h^{-1}$) are very closed in their intrinsic reactivity and essentially more reactive than ZVI1 ($k_{EDTA}$ = 24 ± 1 μg $h^{-1}$). Upon immersion in water $Fe^0$ dissolves to $Fe^{2+}$ (Eq. 5). Under the experimental conditions, $Fe^{II}$ is further oxidized to $Fe^{III}$ (Eq. 6) which solubility at pH > 4.5 is very low. Using a 2.0 mM EDTA solution to form stable complexes with EDTA (Eq. 7) was demonstrated a powerful tool to assess the reactivity of $Fe^0$ [11,31].

$$Fe^0 + 2\ H^+ \Rightarrow Fe^{2+} + H_2 \quad (5)$$

$$Fe^{2+} + ½\ O_2 + H_2O \Rightarrow Fe^{3+} + 2\ HO^- \quad (6)$$

$$Fe^{3+} + EDTA \Rightarrow FeEDTA^{3+} \quad (7)$$

Given the higher stability of $Fe^{III}$-EDTA relative to $Fe^{II}$- EDTA, ascorbic acid was identified a powerful agent for the reduction of the $Fe^{III}$-EDTA prior to Fe determination using the 1,10 orthophenanthroline method [31].

The data in Tab. 4 suggests that the reactivity difference can be attributed to the particle size distribution (material sorting) (Fig. 1). Material intrinsic reactivity is generally influenced by practical considerations including particle size, chemical composition, production and storage conditions [26,46,47]. The single information accessible for the three tested materials is their mean particle diameter (ϕ value - Tab. 4). While the ϕ value is 0.50 mm for ZVI10 [41] and ZVI9, its value for ZVI1 is 0.60 mm. The fact that materials with finer particle size are more

283 reactive than coarser materials is the rationale for the use of nano-scale particles in water
284 treatment [48,49]. However, it should be recalled that the particle size alone is not an
285 indicator for the intrinsic reactivity [18,31,19]. Rigorously, if the particle size distribution of
286 ZVI9 was not given by the supplier, a researcher could have sieved all three materials and
287 used the fraction 0.40 to 0.80 mm as one fraction. In other words, the difference in particle
288 size of used materials is minimal ($\phi$ value). However, the assertion that 'finer particle size are
289 more reactive than coarser materials' is operationally maintained in this study [11,26,31].
290 Remember that the EDTA test is in essence a reactivity test. Characterizing the same material
291 available in different particle sizes can be regarded as validation of the experimental protocol.
292 This has already been performed in previous work [11,31]. The Rheinfelden $Fe^0$ (iPutec
293 GmbH & Co KG) depicted $k_{EDTA}$ values decreasing from 61 ± 6 μg $h^{-1}$ to 27 ± 1 μg $h^{-1}$ when
294 the particle size fraction increased from 0.315 - 0.500 mm to 1.0 - 2.0 mm. In the present
295 work, the lack of significant difference between the reactivity of ZVI1 (0.400 - 0.800 mm)
296 and ZVI4 (0.300 - 2.0 mm) is attributed to the proportion of smaller size particles (0.300 -
297 0.400 mm) in ZVI4 (Fig. 1). This work correlates 'intrinsic reactivity' and 'treatability
298 efficiency' for MB discoloration. The terms 'reactivity' and 'efficiency' are currently
299 confusing in the literature. They are almost always randomly interchanged.

300 **4.3 MB column test**

301 The EDTA test has revealed the following reactivity order for tested materials: ZVI10 ≅ ZVI9
302 >> ZVI1. The present section characterizes the efficiency of tested materials in term of (i)
303 iron release, (ii) MB discoloration and (iii) permeability loss.

304 **4.3.1 Iron release**

305 Fig. 5 summarizes the results of iron release by tested materials during the experiments (30
306 days). It is seen that ZVI9 was the most efficient material followed by ZVI10. ZVI1 was the
307 least efficient material. The cumulative mass of iron in the collected effluent was 18.2 mg for
308 ZVI9, 15.9 mg for ZVI10 and 7.8 mg for ZVI1 (Tab. 4). Accordingly, the efficiency order for

309 Fe release corresponds to the reactivity order after the EDTA test: ZVI9 ≅ ZVI10 >> ZVI1. It
310 is important to notice that the non uniform evolution of Fe release during the first 15 to 20
311 days is a argument against characterizing $Fe^0$ reactivity and efficiency short term experiments
312 [32,33,35]. The observed differential behaviour can be attributed to the presence of fines as
313 ZVI9 and ZVI10 content more fines than ZVI1.

314 **4.3.2 MB discoloration**

315 Fig. 6 summarizes the results of MB discoloration by tested materials during the experiments.
316 Fig. 6a depicts no clear trend in the order of efficiency of the tested materials. For example:
317 (i) for t < 12 d, ZVI9 is clearly the less efficient material; (ii) at day 15, the order of efficiency
318 is ZVI1 > ZVI9 > ZVI10, (iii) at day 25, the corresponding order of efficiency is ZVI10 >
319 ZVI1 > ZVI9. The lack of a clear trend suggest that no (pseudo-) steady state was yet
320 established in the kinetics of $Fe^0$ oxidation coupled with MB discoloration (or its disturbance).
321 In other words, 30 days is too short to graphically differentiate the extent of MB discoloration
322 by tested $Fe^0$ materials using the E value alone.
323 Fig. 6b depicts the time dependant evolution of the mass of MB in the effluent. This is a
324 reflect of the kinetics of the process (iron corrosion) disturbing MB adsorptive discoloration
325 by sand. Fig. 6b clearly shows that MB removal was less efficient in the ZVI9 systems and
326 very comparable in the two other systems (ZVI1 and ZVI10). The derived order of efficiency
327 from Fig. 6b (t > 12 d) is: ZVI1 > ZVI10 > ZVI9. Calculations confirmed that, after 30 days,
328 only 2.8 % of the cumulative mass of MB was collected in the effluent for ZVI1 against 5.6 %
329 for ZVI10 and 11.6 % for ZVI9 (Fig. 6b and 6c).
330 Fig. 6c depicts the time dependant evolution of the cumulative mass of MB in the effluent.
331 The trend from Fig. 6b is confirmed with the additional information that no significant
332 difference can be documented for ZVI1 and ZVI10 for t < 25 d. The graphical order of
333 efficiency from Fig. 6 seems to contradict the order based on Fe release (§ 4.3.1) which is in
334 tune with the reactivity order after the EDTA test.

335 Considering the historical work of Mitchell et al. [36] demonstrating that iron oxide coated
336 sand is a poorer MB adsorbent than pure sand, these results suggest that the most reactive
337 system is the one exhibiting the lowest efficiency for MB discoloration (e.g. ZVI9).
338 Considering this essential aspect, it appears that ZVI1 is the less reactive material as found by
339 Fe release (section 4.3.1) and EDTA test (§ 4.2). Accordingly, Assumption 1 is validated with
340 regard to MB discoloration and Fe release.

341 **4.3.3 Permeability loss**

342 Fig. 7 summarizes the results of the evolution of the hydraulic conductivity (k in mm $min^{-1}$) as
343 a function of the time. A monotone decrease of the k value is observed with the progress of
344 the filtration (Fig. 7a). Fig. 7a also shows that the initial k value ($k_0$ - Tab. 4) was essentially
345 lower for ZVI1 than for ZVI10 and ZVI9. This behaviour is primarily attributed to the
346 material sorting [50-54]. In fact, a packed bed of a better sorted granular material exhibits a
347 greater permeability. In better sorted beds (ZVI10, ZVI9) the pore spaces are open. In the
348 comparatively poorly sorted ZVI1 bed fine grains occupy the pore spaces between coarser
349 grains [50,52].

350 Fig. 7b shows that the evolution of the relative permeability (k in %) was very closed for
351 ZVI10 and ZVI9, confirming that the pore volume in both systems are occupied with a similar
352 kinetics ($k_{EDTA}$ values), namely the kinetics of the process of iron hydroxide production. A
353 more rapid porosity loss is observed in the ZVI1 column. This can only be attributed to the
354 poorer sorting, as ZVI1 is significantly less reactive than ZVI10 and ZVI9 (§ 4.2, 4.3.1 and
355 4.3.2). In fact, precipitation of iron hydroxides from $Fe^0$ corrosion causes cementation of the
356 $Fe^0$ grains and acts to fill the pore spaces (porosity) and interconnectivity of the spaces. Both
357 processes result in more rapid decrease of k values (permeability loss) in the ZVI1 system
358 where $Fe^0$ particles are closer to each other (smaller pore radius). The shape of the particles
359 also significantly influences the evolution of the permeability [53,54]. According to Hayati et

al. [54] spherical particles yield a better porosity than cylindrical ones. ZVI9 is almost spherical, ZVI1 and ZVI10 are more cylindrical but ZVI1 is the least sorted material (Fig. 1). The discussion until now has confirmed that material particle size, material sorting and material geometry all significantly influence the hydraulic conductivity [50,52-54]. In $Fe^0$ beds, in-situ generated iron hydroxides tend to cement initial particles and decrease both porosity and permeability. The present study has presented a reliable method to correlate the intrinsic reactivity and the efficiency of $Fe^0$ materials using MB discoloration in column studies (assumption 1 is validated by experimental results). Future research should focus on how the characteristics of $Fe^0$ and admixing additives (e.g. gravel, $MnO_2$, pumice, sand) impact system's sustainability.

Pure $Fe^0$ beds as tested here are not sustainable [1,39]. Admixing additives are natural materials which are rarely uniform in geometry. Accordingly, when mixed with the same additive (e.g. sand), the sustainability of the resulted $Fe^0$/sand systems should be individually tested/discussed. In particular, not the most reactive material/system should be constantly sought, but the material with the most appropriate efficiency. For example, ZVI1 could be more suitable for groundwater remediation and ZVI9 and ZVI10 for wastewater treatment. Alternatively, ZVI1 mixed with a certain material A (size, form, shape) could be suitable for drinking water and the mixture with a second material suitable for wastewater treatment.

### 4.4 Discussion

The thermodynamic instability of $Fe^0$ ($E^0$ = -0.44 V) in water ($E^0$ = 0.00 V) does not provide any information on the kinetics of the corrosion process, which defines the intrinsic reactivity of individual materials. $Fe^0$ reactivity is influenced by material-dependant considerations such as (i) the material elemental composition, (ii) its particle size, (iii) its production and storage conditions. Regarding the test conditions, used operational parameters should be rationally selected to be relevant for field conditions. Relevant operational parameters include (i) used $Fe^0$ amounts, (ii) used $Fe^0$:solution ratios, (iii) used flow rate or mixing intensities, (iv) nature

386 of model contaminants and (v) solution pH. The present study and related works have
387 demonstrated the suitability of MB to enable the differentiation of '$Fe^0$ efficiency' and '$Fe^0$
388 reactivity', regardless of whether these differences are due to elemental composition, particle
389 size or production and storage conditions. The reactivity results for nine commercial $Fe^0$
390 materials including the most used worldwide (e.g. Peerles, Connelly, Rheinfelden) are
391 presented for the first time and could help to comparatively discuss results from independent
392 studies.
393 The consistency among results from two different tests (EDTA and MB) indicates that a
394 standard protocol is urgently needed for the characterization of existing and newly
395 manufactured materials. In particular, material selection for each application should be
396 justified by the efficiency under the specific conditions. Despite 20 years intensive research,
397 the intrinsic reactivity of $Fe^0$ material has not been properly addressed.
398 Because of this technical deficit a real race for the most reactive material was initiated.
399 Resulting materials included bimetallic particles [55], nanoscale particles [48] and some
400 proprietary materials like CIM (Composite Iron Matrix) [1,39], SIM (Sulfur Modified Iron)
401 [56]. However, not always the most reactive material is needed but the most appropriate one.
402 As an example, ZVI8 which is the least reactive material in this study (EDTA test) has been
403 shown more efficient than 3 other more reactive $Fe^0$ materials for As removal under
404 conditions where rapid dissolution kinetics favoured $Fe^0$ 'passivation' [35]. The most
405 appropriate material for a given situation is the one producing enough contaminant scavengers
406 per unit time to achieve the design goal. That is the material which intrinsic reactivity matches
407 the field situation (e.g. water flow rate, nature of the contaminant) the most.
408 **4.4.1 Efficiency and reactivity of $Fe^0$**
409 A rigorous differentiation between 'reactivity' and 'efficiency' is of crucial importance for the
410 future of the use of $Fe^0$ materials for water treatment and environmental remediation. In fact,

411 many reported discrepancies originated from the ill-definition of these two terms. Three
412 examples will be given for illustration:
413 First, Bi et al. [57] found 'paradoxical' that a 85:15 $Fe^0$:sand (w/w) mixture was more
414 efficient for TCE removal than a pure $Fe^0$ system (100 % $Fe^0$). In both systems, the $Fe^0$
415 reactivity is the same (invariable) but the efficiency of the $Fe^0$/sand system is increased thanks
416 to the presence of non-expansive sand (delayed clogging or extended $Fe^0$ depletion) [37].
417 Second, For the same $Fe^0$, Ruhl et al. [30] reported on differential averaged corrosion rates in
418 shorter and longer columns. The corrosion rate, assessed by the extent of $H_2$ generation, was
419 reported higher in shorter columns. It is obvious that the authors confounded the efficiency of
420 the systems for $H_2$ release and the iron corrosion rate. The corrosion rate, as an invariable
421 intrinsic characteristic of the used $Fe^0$ material. It is the same for all columns (same $Fe^0$
422 material). The measured volume of $H_2$ depends on the extends of hindrance within individual
423 columns. Generated $H_2$ must migrate through the $Fe^0$ column and only the escaped fraction is
424 measured. Disregarding the nature of hindrances in the $Fe^0$ columns, the results of Ruhl et al.
425 [30] are better explained by the deep-bed nature of filtration on $Fe^0$ columns. It is therefore
426 traceable that less $H_2$ escapes from a higher column.
427 Third, Ruhl and Jekel [26] found out that the grain size distribution of a $Fe^0$ material affects
428 "the porosity, the pore geometry and the reactivity". It is evident that 'reactivity' here is
429 referred to 'removal efficiency' as it is further stated that 'column tests showed that all
430 fractions achieved good TCE removal with a slight advantage for smaller grains'. However,
431 assuming cylindrical porous structure, the pore radius for smaller grains is narrow and should
432 be rapidly filled/clogged by the more reactive small particles. In other words, reactive zones
433 with smaller grain sizes are more susceptible to clogging. The discussion of Ruhl and Jekel
434 [26] could be optimised. For the discussion herein, however, it is sufficient to consider that
435 purposefully distinguishing between 'reactivity' and 'efficiency' would have impacted the
436 experimental design and/or enabled a stronger discussion with the presented material.

The proper consideration of the expansive nature of iron corrosion suggests that a $Fe^0$-based filter should be regarded as a classical self-filtration system [58]. The processes of (i) $Fe^0$ dissolution, (ii) migration and rearrangement of in-situ generated Fe species and (iii) removal of inflowing foreign species (including contaminants) within the porous medium are central to the understanding of pore clogging and filter design. Presently, the clogging process of $Fe^0$ filters is still poorly understood [16]. The present work and related studies [59-61] suggest that this issue was even not properly addressed.

## 5 Concluding remarks

The suitability and the reliability of a 2.0 mg $L^{-1}$ methylene blue (MB) solution to correlate $Fe^0$ intrinsic reactivity and $Fe^0$ efficiency for MB discoloration in column studies was established. This work shows conclusively that the MB efficiency test yields reliable results to investigate the process permeability loss in $Fe^0$ columns. The major recommendation is that well-sorted materials should be used for sustainable (long term permeable) $Fe^0$ filtration systems. In particular, bulk Rheinfelden materials (0.3 to 2.0 mm) should be fractionated in several fractions, each fraction being probably appropriate for a different goal, e.g. coarser fraction for pre-filtration or $O_2$ scavenging. Further investigations should focus at characterizing the effect of particle shape and size of $Fe^0$ and non-expansive additives (e.g. gravel, pumice, sand) on the process of permeability loss. Virtually, every aspect of contaminant removal in $Fe^0$ beds could be addressed by a purposeful modified protocol.

One of the most important challenges is now to use this basic scientific knowledge to improve the efficiency of the '$Fe^0$ technology' as a whole [59-61]. The acquirement of reliable results and their dissemination will also impact public awareness and acceptance this promising technology. Upon a science-based acceptance, networking between scientists, industrials, end-users and governmental authorities will be promoted in order to ensure successful large scale implementation of the promising '$Fe^0$ technology' for groundwater remediation, wastewater treatment and safe drinking water provision.

**Acknowledgements**

For providing the iron materials investigated in this study the authors would like to express their gratitude to iPutec GmbH (Rheinfelden, Germany), Ann-Marie Gottinger from Mainstream Water Solutions Inc. (Regina, Canada) and Paolo S. Calabrò from the University Calabria (Italy). Mohammed Saad (Leesu, Ecole des Ponts ParisTech, Marne La Vallée), Mehmet A. Oturan and Hugo Gonzales (LGE, Institute IFI, Marne la Vallée) are thanked for their help, their grateful discussion and the possibility to use their spectrophotometer. Tanja Stegemann (Geoscience Museum – University of Göttingen) is acknowledged for the micrographs. This work was partly supported by the "Service de Coopération et d'Action Culturelle" (SCAC) from the France Embassy in Yaoundé (Cameroun).

**References**

[1] A. Hussam, Contending with a development disaster: SONO filters remove arsenic from well water in Bangladesh, Innovations 4 (2009) 89–102.

[2] S. Comba, A. Di Molfetta, R. Sethi, A Comparison between field applications of nano-, micro-, and millimetric zero-valent iron for the remediation of contaminated aquifers, Water Air Soil Pollut. 215 (2011) 595–607.

[3] M. Gheju, Hexavalent chromium reduction with zero-valent iron (ZVI) in aquatic systems, Water Air Soil Pollut. 222 (2011) 103–148.

[4] D.E. Giles, M. Mohapatra, T.B. Issa, S. Anand, P. Singh, Iron and aluminium based adsorption strategies for removing arsenic from water, J. Environ. Manage. 92 (2011) 3011–3022.

[5] C. Noubactep, Metallic iron for safe drinking water worldwide, Chem. Eng. J. 165 (2010) 740–749.

[6] C. Noubactep, Metallic iron for safe drinking water production, Freiberg Online Geol. 27 (2011) 38 pp, ISSN 1434-7512. (www.geo.tu-freiberg.de/fog).

488 [7] ITRC (Interstate Technology & Regulatory Council) *Permeable Reactive Barrier:*
489 *Technology Update*. PRB-5. Washington, D.C.: Interstate Technology & Regulatory
490 Council, PRB: Technology Update Team. www.itrcweb.org (2011) (access:
491 29.04.2012).
492 [8] R.L. Landis, R.W. Gillham, E.J. Reardon, R. Fagan, R.M. Focht, J.L. Vogan, An
493 examination of zero-valent iron sources used in permeable reactive barriers. 3rd
494 International Containment Technology Conference (10-13 June 2001), Florida State
495 University, Tallahassee. Orlando, FL. (2001) 5 pages.
496 [9] R. Miehr, G.P. Tratnyek, Z.J. Bandstra, M.M. Scherer, J.M. Alowitz, J.E. Bylaska,
497 Diversity of contaminant reduction reactions by zerovalent iron: Role of the reductate,
498 Environ. Sci. Technol. 38 (2004) 139–147.
499 [10] O.X. Leupin, S.J. Hug, Oxidation and removal of arsenic (III) from aerated groundwater
500 by filtration through sand and zero-valent iron, Wat. Res. 39 (2005) 1729–740.
501 [11] C. Noubactep, T. Licha, T.B. Scott, M. Fall, M. Sauter, Exploring the influence of
502 operational parameters on the reactivity of elemental iron materials, J. Hazard. Mater.
503 172 (2009) 943–951.
504 [12] M. Gheju, I. Balcu, Hexavalent chromium reduction with scrap iron in continuous-flow
505 system. Part 2: Effect of scrap iron shape and size, J. Hazard. Mater. 182 (2010) 484–
506 493.
507 [13] G. Bartzas, K. Komnitsas, I. Paspaliaris, Laboratory evaluation of $Fe^0$ barriers to treat
508 acidic leachates, Miner. Eng. 19 (2006) 505–514.
509 [14] G. Bartzas, K. Komnitsas, Solid phase studies and geochemical modelling of low-cost
510 permeable reactive barriers, J. Hazard. Mater. 183 (2010) 301–308.
511 [15] L. Li, C.H. Benson, Evaluation of five strategies to limit the impact of fouling in
512 permeable reactive barriers, J. Hazard. Mater. 181 (2010) 170–180.

513 [16] A.D. Henderson, A.H. Demond, Impact of solids formation and gas production on the
514 permeability of ZVI PRBs, J. Environ. Eng. 137 (2011) 689–696.
515 [17] S.-W. Jeen, R.T. Amos, D.W. Blowes, Modeling gas formation and mineral precipitation
516 in a granular iron column, Environ. Sci. Technol. 46 (2012) 6742–6749.
517 [18] R.A. Crane, T.B. Scott, Nanoscale zero-valent iron: Future prospects for an emerging
518 water treatment technology, J. Hazard. Mater. 211–212 (2012) 112–125.
519 [19] C. Noubactep, S. Caré, R.A. Crane, Nanoscale metallic iron for environmental
520 remediation: prospects and limitations, Water Air Soil Pollut. 223 (2012) 1363–1382.
521 [20] Q.-G. Chang, W. Zhang, W.-X. Jiang, B.-J. Li, W.-C. Ying, W. Lin, Efficient micro
522 carbon column rapid breakthrough technique for water and wastewater treatability
523 studies, Environ. Progr. 26 (2007) 280–288.
524 [21] E.M. Pierce, D.M. Wellman, A.M. Lodge, E.A. Rodriguez, Experimental determination
525 of the dissolution kinetics of zero-valent iron in the presence of organic complexants,
526 Environ. Chem. 4 (2007) 260–270.
527 [22] V. Tanboonchuy, N. Grisdanurak, C.H. Liao, Background species effect on aqueous
528 arsenic removal by nano zero-valent iron using fractional factorial design, J. Hazard.
529 Mater. 205-206 (2012) 40–46.
530 [23] C. Noubactep, A. Schöner, P. Woafo, Metallic iron filters for universal access to safe
531 drinking water, Clean: Soil, Air, Water 37 (2009) 930–937.
532 [24] M. Kubare, J. Haarhoff, Rational design of domestic biosand filters, J. Water Supply:
533 Res. Technol. – AQUA 59 (2010) 1–15.
534 [25] A.S. Ruhl, N. Ünal, M. Jekel, Evaluation of two-component Fe(0) fixed bed filters with
535 porous materials for reductive dechlorination, Chem. Eng. J. 209 (2012) 401–406.
536 [26] A.S. Ruhl, M. Jekel, Impacts of Fe(0) grain sizes and grain size distributions in
537 permeable reactive barriers, Chem. Eng. J. 213 (2012) 245–250.

538 [27] J.E. Reardon, Anaerobic corrosion of granular iron: Measurement and interpretation of
539 hydrogen evolution rates, Environ. Sci. Technol. 29 (1995) 2936–2945.
540 [28] J.E. Reardon, Zerovalent irons: Styles of corrosion and inorganic control on hydrogen
541 pressure buildup, Environ. Sci. Tchnol. 39 (2005) 7311–7317.
542 [29] J.E. Reardon, R. Fagan, J.L. Vogan, A. Przepiora, Anaerobic corrosion reaction kinetics
543 of nanosized iron, Environ. Sci. Technol. 42 (2008) 2420–2425.
544 [30] A.S. Ruhl, A. Weber, M. Jekel, Influence of dissolved inorganic carbon and calcium on
545 gas formation and accumulation in iron permeable reactive barriers, J. Contam.
546 Hydrol. 142–143 (2012) 22–32.
547 [31] C. Noubactep, G. Meinrath, P. Dietrich, M. Sauter, B. Merkel, Testing the suitability of
548 zerovalent iron materials for reactive walls, Environ. Chem. 2 (2005) 71–76.
549 [32] C. Noubactep, Characterizing the reactivity of metallic iron in $Fe^0/EDTA/H_2O$ systems
550 with column experiments, Chem. Eng. J. 162 (2010) 656–661.
551 [33] C. Noubactep, Characterizing the reactivity of metallic iron in $Fe^0/U^{VI}/H_2O$ systems by
552 long-term column experiments, Chem. Eng. J. 171 (2011) 393–399.
553 [34] C. Noubactep, Characterizing the reactivity of metallic iron upon methylene blue
554 discoloration in $Fe^0/MnO_2/H_2O$ systems, J. Hazard. Mater. 168 (2009) 1613–1616.
555 [35] C. Noubactep, Characterizing the reactivity of metallic iron in $Fe^0$/As-rock/$H_2O$ systems
556 by long-term column experiments, Water SA 38 (2012) 511–517.
557 [36] G. Mitchell, P. Poole, H.D. Segrove, Adsorption of methylene blue by high-silica sands,
558 Nature 176 (1955) 1025–1026.
559 [37] C. Noubactep, S. Caré, F. Togue-Kamga, A. Schöner, P. Woafo, Extending service life of
560 household water filters by mixing metallic iron with sand, Clean – Soil, Air, Water 38
561 (2010) 951–959.

562 [38] C. Noubactep, S. Caré, K.B.D. Btatkeu, C.P. Nanseu-Njiki, Enhancing the sustainability
563 of household $Fe^0$/sand filters by using bimetallics and $MnO_2$, Clean – Soil, Air, Water
564 40 (2012) 100–109.
565 [39] A. Hussam, A.K.M. Munir, A simple and effective arsenic filter based on composite iron
566 matrix: Development and deployment studies for groundwater of Bangladesh, J.
567 Environ. Sci. Health A 42 (2007) 1869–1878.
568 [40] K. Miyajima, C. Noubactep, Effects of mixing granular iron with sand on the efficiency
569 of methylene blue discoloration, Chem. Eng. J. 200–202 (2012) 433–438.
570 [41] A.M. Gottinger, Chemical-free arsenic removal from potable water with a ZVI-amended
571 biofilter. Master thesis, University of Regina (Saskatchewan, Canada), (2010) 90 pp.
572 [42] J. Pietsch, W. Schmidt, F. Sacher, S. Fichtner, H. Brauch, Pesticides and another organic
573 micropollutants in the river Elbe, Fresenius J. Anal. Chem. 353 (1995), 75–82.
574 [43] H. Chiew, M.L. Sampson, S. Huch, S. Ken, B.C. Bostick, Effect of groundwater iron and
575 phosphate on the efficacy of arsenic removal by iron-amended biosand filters,
576 Environ. Sci. Technol. 43 (2009) 6295–6300.
577 [44] W.B. Fortune, M.G. Mellon, Determination of iron with o-phenanthroline: a
578 spectrophotometric study, Ind. Eng. Chem. Anal. Ed. 10 (1938) 60–64.
579 [45] L.G. Saywell, B.B. Cunningham, Determination of iron: colorimetric o-phenanthroline
580 method, Ind. Eng. Chem. Anal. Ed. 9 (1937) 67–69.
581 [46] H.S. Salem, G.V. Chilingarian, The cementation factor of Archie's equation for shaly
582 sandstone reservoirs, J. Pet. Sci. Eng. 23 (1999) 83–93.
583 [47] J.H. Potgieter, S.S. Potgieter, S.J. Moja, A. Mulaba-Bafubiandi, The standard reactivity
584 test as a measure of lime's quality, J. South African Inst. Mining Metal.
585 January/February 2002 (2002) 67–69.
586 [48] C.B. Wang, W.-X. Zhang, Synthesizing nanoscale iron particles for rapid and complete
587 dechlorination of TCE and PCBs, Environ. Sci. Technol. 31 (1997) 2154–2156.

588 [49] C. Macé, S. Desrocher, F. Gheorghiu, A. Kane, M. Pupeza, M. Cernik, P. Kvapil, R.
589 Venkatakrishnan, W.-X. Zhang, Nanotechnology and groundwater remediation: A
590 step forward in technology understanding, Remed. J. 16 (2006) 23–33.
591 [50] C.W. Fetter, *Applied Hydrogeology*, 3rd ed. Upper Saddle River, NJ: Prentice Hall, Inc
592 (1994).
593 [51] R.P. Dias, J.A. Teixeira, M.G. Mota, A.I. Yelshin, Particulate binary mixtures:
594 Dependence of packing porosity on particle size ratio, Ind. Eng. Chem. Res. 43 (2004)
595 7912–7919.
596 [52] R.P. Dias, C.S. Fernandes, J.A. Teixeira, M. Mota, A. Yelshin, Permeability analysis in
597 bisized porous media: Wall effect between particles of different size, J. Hydrol. 349
598 (2008) 470–474.
599 [53] M.M. Ahmadi, S. Mohammadi, A.N. Hayati, Analytical derivation of tortuosity and
600 permeability of monosized spheres: A volume averaging approach, Phys. Rev. E 83
601 (2011) 026312 [8 pages].
602 [54] A.N. Hayati, M.M. Ahmadi, S. Mohammadi, How particle shape affects the flow through
603 granular materials, Phys. Rev. E 85, 036310 (2012) [4 pages].
604 [55] R. Muftikian, Q. Fernando, N. Korte, A method for the rapid dechlorination of
605 lowmolecularweight chlorinated hydrocarbons inwater, Water Res. 29 (1995) 2434–
606 2439.
607 [56] B.J. Allred, Laboratory evaluation of zero valent iron and sulfur-modified iron for
608 agricultural drainage water treatment, Ground Water Monit. Remed. 32 (2012) 81–95.
609 [57] E. Bi, J.F. Devlin, B. Huang, Effects of mixing granular iron with sand on the kinetics of
610 trichloroethylene reduction, Ground Water Monit. Remed. 29 (2009) 56–62.
611 [58] O. Dikinya, C. Hinz, G. Aylmore, Decrease in hydraulic conductivity and particle release
612 associated with self-filtration in saturated soil columns, Geoderma 146 (2008) 192–
613 200.

614 [59] C. Noubactep, Aqueous contaminant removal by metallic iron: Is the paradigm shifting?
615 Water SA 37 (2011) 419–426.
616 [60] R. Crane, C. Noubactep, Elemental metals for environmental remediation: learning from
617 hydrometallurgy, Fresenius Environ. Bull. 21 (2012) 1192–1196.
618 [61] S. Caré, R. Crane, P.S. Calabro, A. Ghauch, E. Temgoua, C. Noubactep, Modelling the
619 permeability loss of metallic iron water filtration systems, Clean – Soil, Air, Water
620 (2012) doi: 10.1002/clen.201200167.
621

621 **Table 1**: Column tests program. One use cycle consists of a filtration period, followed by a
622 resting period with no flow. As expansive corrosion induces permeability loss, the
623 filtration period will become longer. The test program can regarded as the
624 investigation of the impact of a ca. 5 cm layer of $Fe^0$ on the discoloration ability of
625 a 2.0 mg $L^{-1}$ MB solution.

626

| **material** | **size** (mm) | **code** | **high** (cm) | **mass** (g) | **function** |
|---|---|---|---|---|---|
| **solution** | - | $H_{solution}$ | 15.5 | (-) | resting solution |
| **coarse sand** | 1.6 - 2.0 | $H_1$-sand | 19.1 - 20.0 | 172.4 | lower MB adsorbent |
| **$Fe^0$** | 0.3 - 2.0 | $H_{iron}$ | 4.5 – 5.4 | 100.0 | tested material |
| **fine sand** | 0.25-0.30 | $H_2$-sand | 8.0 | 60.0 | stronger MB adsorbent |

627
628
629
630

630 **Table 2**: Origin, name and main characteristics of tested $Fe^0$ materials.

631

| origin | original denotation | code | form | ∅ (μm) [(a)] |
|---|---|---|---|---|
| **iPutec GmbH** | FG 0300/2000 | ZVI1 | filings | 400-800 |
| **G. Maier GmbH** | FG 0300/2000 | ZVI2 | filings | 300-2000 |
| **Connelly-GPM** | ETC-CC-1004 | ZVI3 | filings | 1000-3000 |
| **iPutec GmbH** | FG 0300/2000 | ZVI4 | filings | 300-3000 |
| **G. Maier GmbH** | Graugußgranulat | ZVI5 | chips | 350-1200 |
| **Connelly-GPM** | ETC-CC-1004 | ZVI6 | filings | 500-1000 |
| **MAZ, mbH** | Sorte 69[(b)] | ZVI7 | filings | 80-4000 |
| **Würth** | Hartgußstrahlmittel | ZVI8 | spherical | 1200 |
| **Pometon S.p.A.** | Ferblast RI 850 | ZVI9 | filings | 500 |
| **Peerless Metals** | Unknown | ZVI10 | filings | 450-550 [(c)] |

632 [(a)] Average values from material supplier; [(b)] Scrap iron material, [(c)] values from ref. [41].

633

634

635

635 **Table 3**: Corresponding correlation parameters ($k_{EDTA}$, b) for the 10 metallic iron materials.
636 As a rule, the more reactive a material is under given conditions the larger the $k_{EDTA}$
637 value. General conditions: initial pH 5.2, initial EDTA concentration 2 mM, room
638 temperature 23 ± 2 °C, and $Fe^0$ mass loading 2 g $L^{-1}$. $k_{EDTA}$ and b-values were
639 calculated in Origin 6.0. "n.d." stands for not determined.
640

| **Material** | **Origin** | **$k_{EDTA}$** (μg/h) | **b** (μg) |
|---|---|---|---|
| **ZVI1** | iPutec | 24 ± 1 | 136 ± 15 |
| **ZVI2** | G.M.GmbH | 29 ± 1 | 117 ± 15 |
| **ZVI3** | Connelly | 32 ± 1 | 193 ± 25 |
| **ZVI4** | iPutec | 23 ± 1 | 73 ± 9 |
| **ZVI5** | G.M.GmbH | 27 ± 1 | 108 ± 10 |
| **ZVI6** | Connelly | 24 ± 4 | 1685 ± 289 |
| **ZVI7** | MAZ, mbH | 27 ± 1 | 173 ± 13 |
| **ZVI8** | Würth | 13 ± 1 | 65 ± 20 |
| **ZVI9** | FERBLAST | 36 ± 3 | 185 ± 69 |
| **ZVI10** | Peerless | 37 ± 2 | 210 ± 159 |

641
642
643
644

644 **Table 4**: Results of the $Fe^0$ characterization in batch ($k_{EDTA}$) and column experiments. $v_0$ is
645 the initial flow velocity, $[Fe]_0$ the level of dissolved iron after 4 days, $\Sigma[Fe]$ the total
646 mass of leached Fe, $\Sigma[MB]_f$ the cumulative extent of MB dicoloration and $k_{EDTA}$ the
647 dissolution kinetics of $Fe^0$ in 2 mM EDTA. It should be noticed that less than 0.02 %
648 of the initial amount of $Fe^0$ (100 g) has been leached during the experiment.

649
650

| **Material** | **Size** (mm) | **$k_0$** (mm $min^{-1}$) | **$[Fe]_0$** (mg $L^{-1}$) | **$\Sigma[Fe]_f$** (mg) | **E** (%) | **$k_{EDTA}$** (mg $h^{-1}$) |
|---|---|---|---|---|---|---|
| **ZVI1** | 0.40 - 0.80 | 7.7 | 2.7 | 8.0 | 97.2 | 24 ± 1 |
| **ZVI10** | 0.45 - 0.55 | 43.2 | 1.4 | 15.9 | 94.4 | 37 ± 2 |
| **ZVI9** | 0.50 | 44.4 | 2.2 | 18.2 | 88.4 | 36 ± 3 |

651
652

**Figure 1**

ZVI 1 (iPutec GmbH)

ZVI 2 (Gotthart Mayer GmbH)

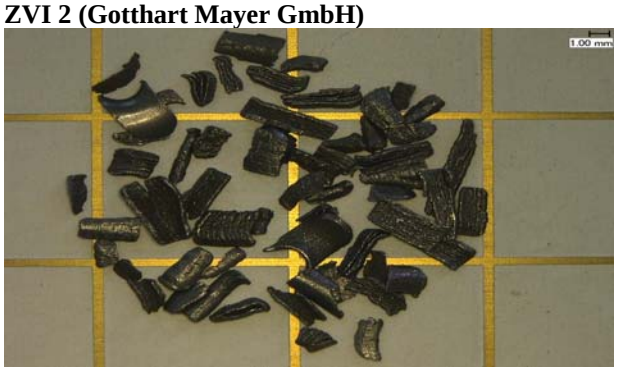

ZVI 3 (Connelly iron GPM)

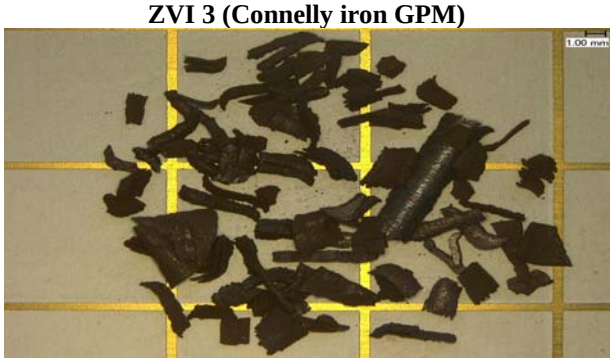

ZVI 4 (iPutec GmbH)

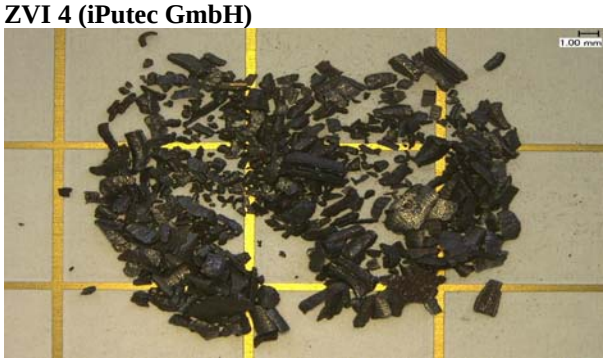

ZVI 5 (Gotthart Mayer GmbH)

ZVI 6 (Connelly iron GPM)

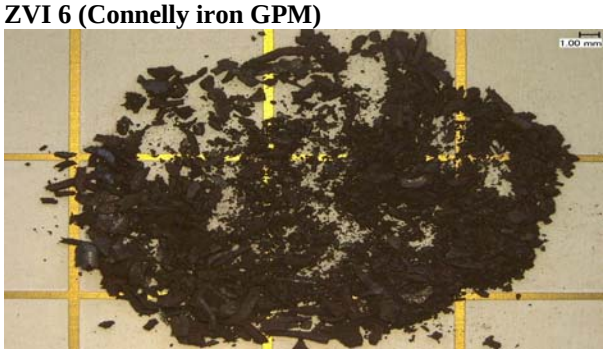

ZVI 7 (MAZ, mbH)

ZVI 8 (Würth)

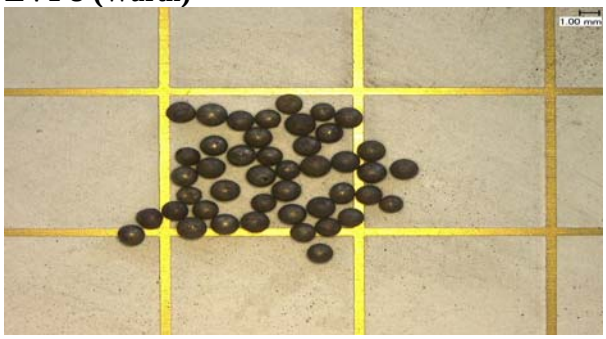

ZVI 9 (Ferblast)

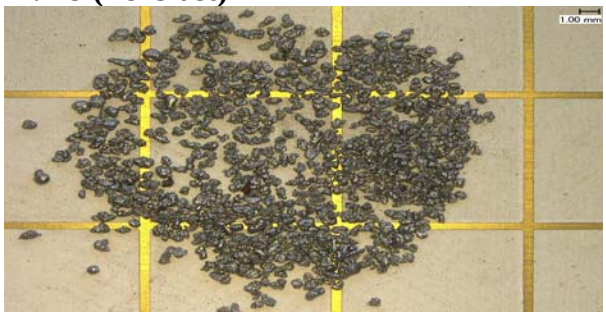

ZVI 10 (Peerless)

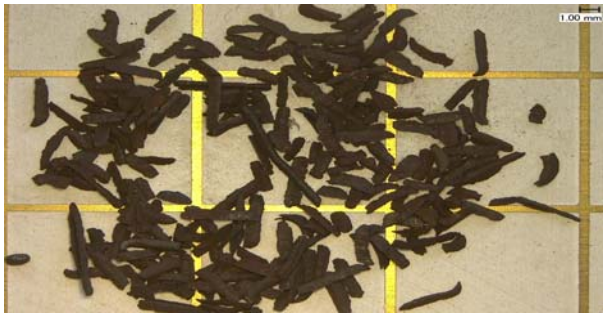

654 **Figure 2**

655

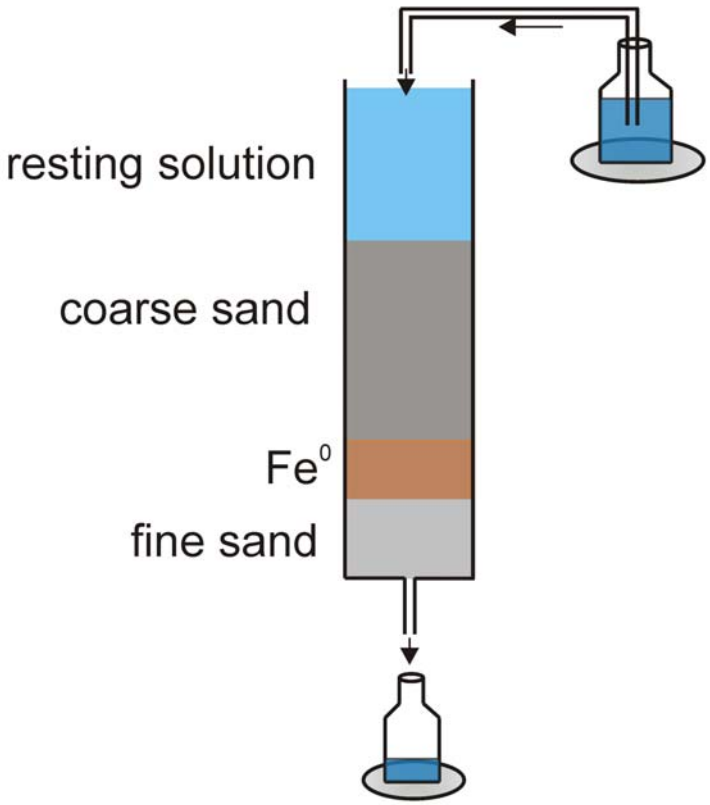


656

657

658

**Figure 3**

**ZVI 1**

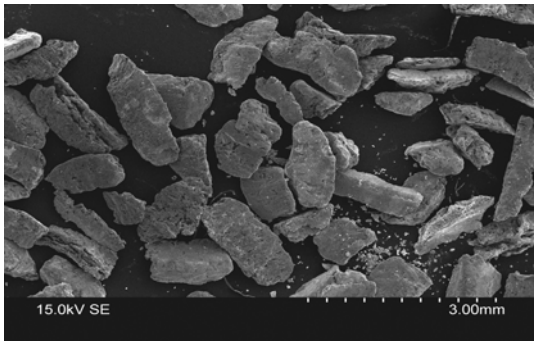


**ZVI9**

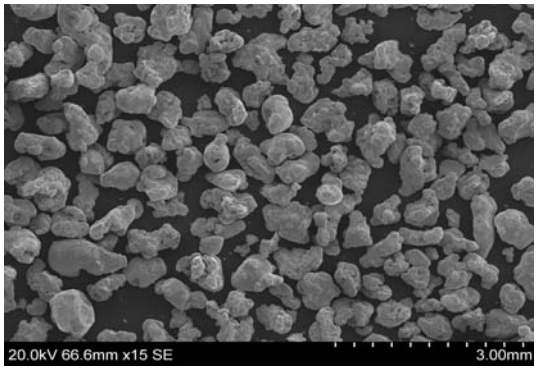


**ZVI 10**

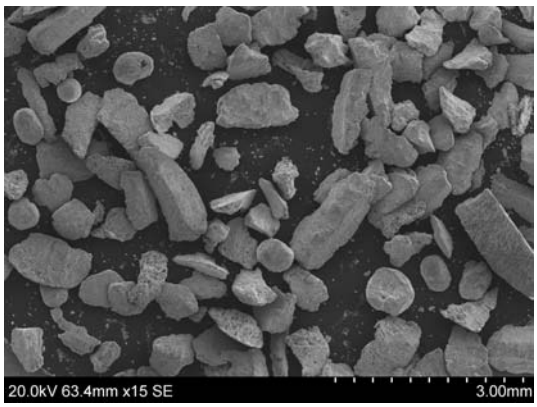


**Sand**

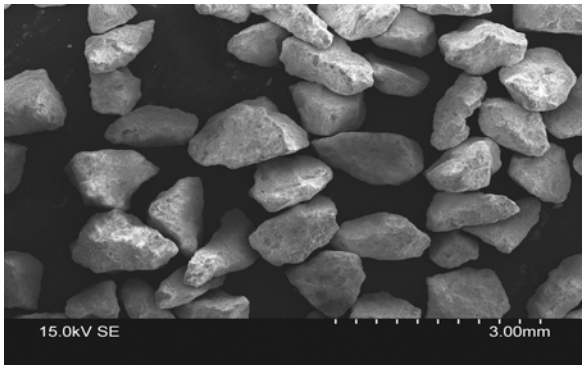

681 **Figure 4**

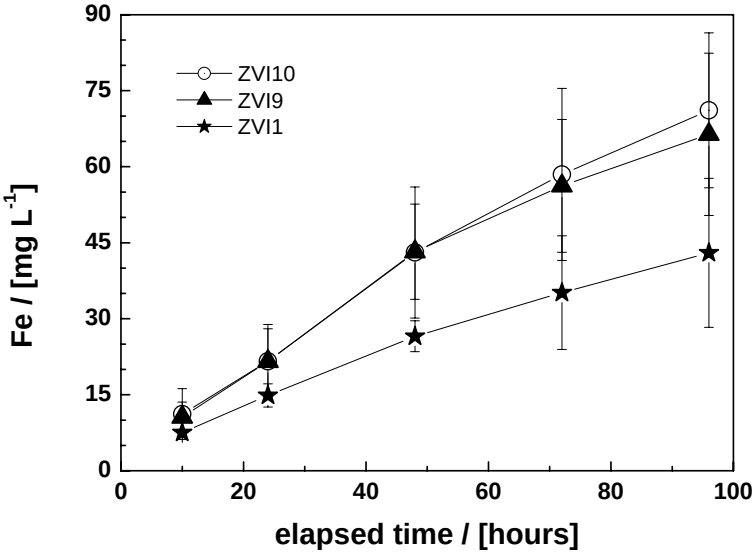


682

683

683 **Figure 5**

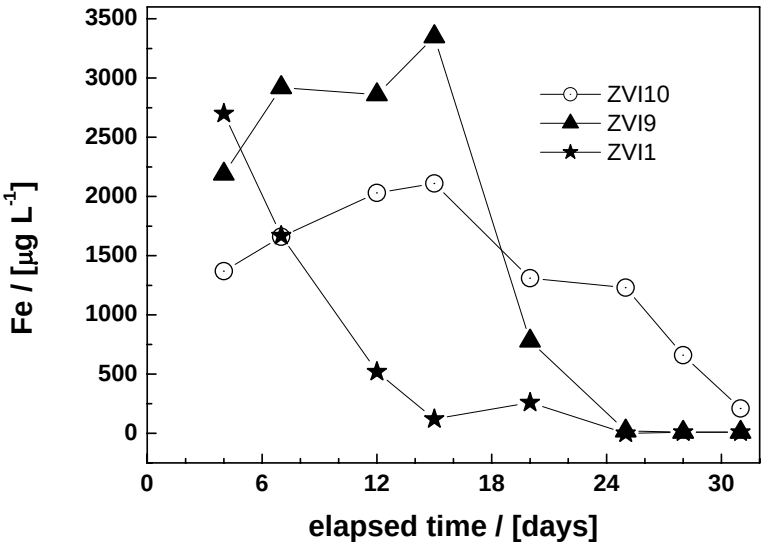


684

685

686

686 **Figure 6**

687

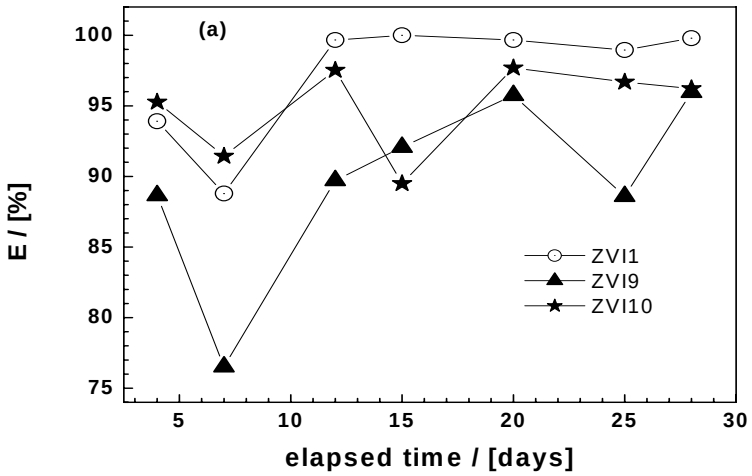


688

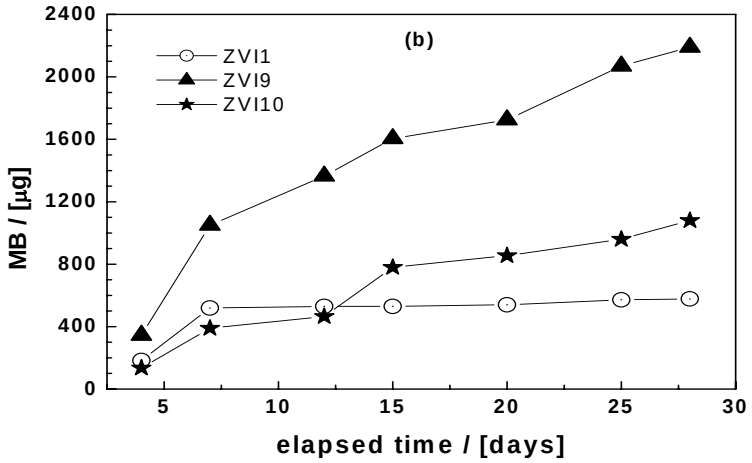


689

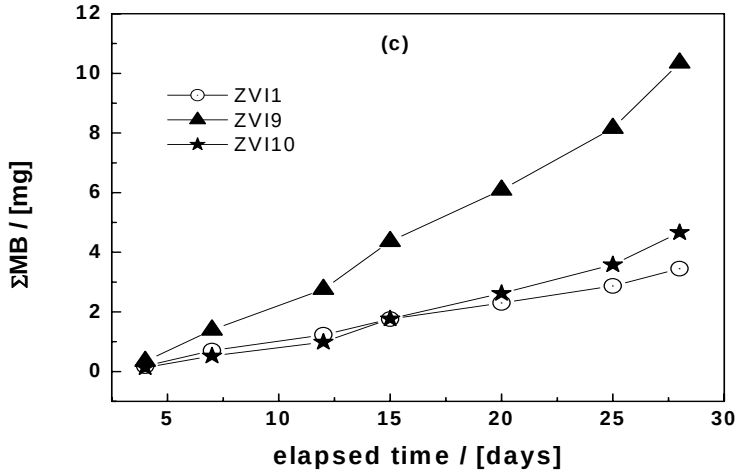


690

691

691 **Figure 7**

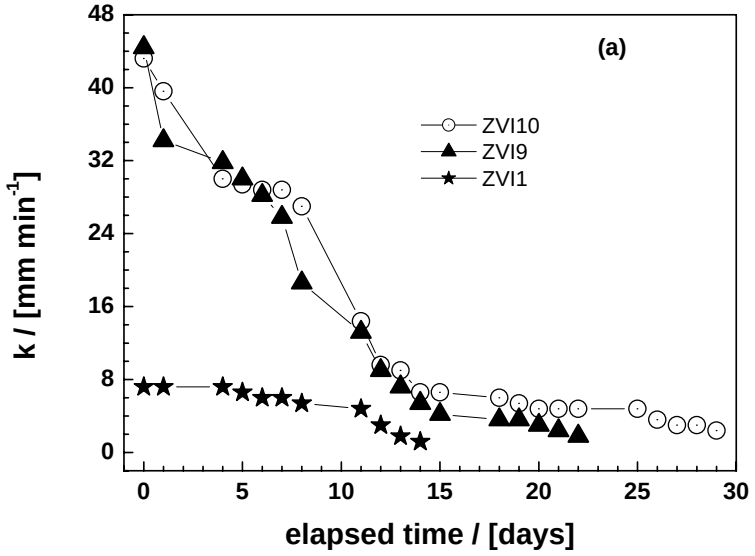


692

693

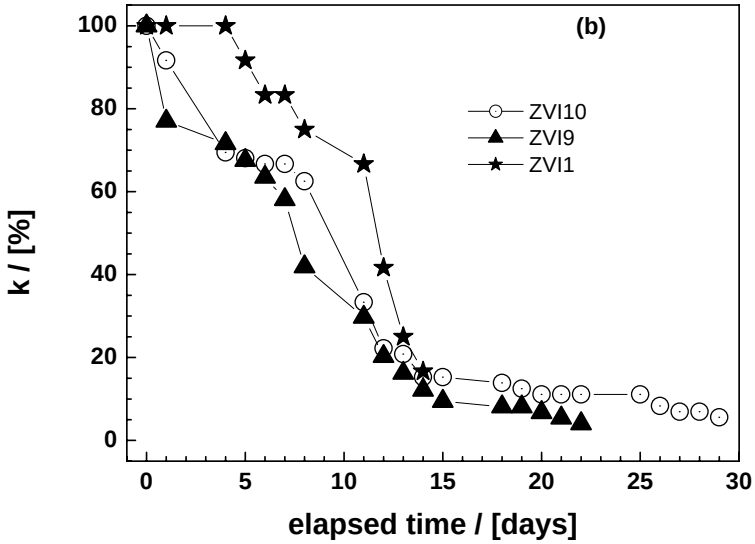


694

695

695 **Figure captions**

696 **Figure 1:** Micrographs of the then tested granulated metallic iron materials. Distances of lines
697 in the background are 1 cm in vertical and horizontal directions. 500 mg of each material was
698 used.

699

700 **Figure 2:** Schematic diagram of the experimental design. Due to the volumetric expansive
701 nature of aqueous iron corrosion ($Fe^0$), progressive increase in the filtration time during use
702 (permeability loss) is expected.

703

704 **Figure 3**: SEM images of the material particles used in column experiments: sand, ZVI1,
705 ZVI9 and ZVI10.

706

707 **Figure 4:** Iron dissolution from the three $Fe^0$ materials by 2 mM EDTA under non-disturbed
708 conditions for four days. Error bars denote the standard error for triplicate experimental
709 results. The lines are not fitting functions, they simply connect points to facilitate
710 visualization.

711

712 **Figure 5:** Evolution of the dissolved iron concentration in the effluent as a function of time.
713 Experimental conditions: 100 g $Fe^0$ representing about 5 cm of a material layer; [MB] = 2.0
714 mg $L^{-1}$. Filling material: sand. Column length 50 cm, column diameter 2.6 cm. The lines are
715 not fitting functions, they simply connect points to facilitate visualization.

716

717 **Figure 6:** Evolution of the extent of methylene blue (MB) discoloration by $Fe^0$ as a function
718 of time: (a) E values, (b) mass of MB in the effluent, and (c) cumulative mass of MB in the
719 effluent. Experimental conditions: 100 g $Fe^0$ representing about 5 cm of a material layer;

720 [MB] = 2.0 mg $L^{-1}$. Filling material: sand. Column length 50 cm, column diameter 2.6 cm.
721 The lines are not fitting functions, they simply connect points to facilitate visualization.
722
723 **Figure 7:** Evolution of the hydraulic conductivity (permeability) by $Fe^0$ column as a function
724 of time: (a) absolute permeability, and (b) relative permeability. Experimental conditions: 100
725 g $Fe^0$ representing about 5 cm of a material layer; [MB] = 2.0 mg $L^{-1}$. Filling material: sand.
726 Column length 50 cm, column diameter 2.6 cm. It can be seen that after 12 days the initial
727 permeability has decreased by more than 80 % in all systems. The lines are not fitting
728 functions, they simply connect points to facilitate visualization.